Intel International Science and Engineering Fair

Natural Characteristics That Lead to Superhydrophobicity

SBI168

Biology

Jason Wu

Table of Contents:

1. Abstract:

Nature has figured out a way to create hydrophobic surfaces. Different types of well-developed superhydrophobic and water-repellent surfaces are found in many plant species. Almost all of them have microscale roughness, which is generated by a thin layer of wax coating the underlying papilla-like cells. The objective of this research is to determine how the surface morphology of various plant surfaces affect their hydrophobicity. The contact angle (CA) of water droplets on various plant surfaces are used to quantify and characterize the hydrophobicity of the surfaces. Using scanning electron microscopy (SEM), the microstructures of the flower petals are analyzed. The relationships between hydrophobicity and various surface parameters obtained from SEM images are generated and validated by the Cassie-Baxter and Wenzel solid-liquid-air contact Equation. This investigation paves way for imitating hydrophobic plant surfaces and manufacturing hydrophobic materials for various applications. The study of such properties will be further developed into the construction of the best model for hydrophobic surfaces and materials.

2. Introduction

i. Superhydrophobicity

Superhydrophobic surfaces are of tremendous interest for industrial and technological applications due to their excellent water-repellent properties. For instance, rain gears and exterior walls for buildings are two of the daily uses of hydrophobic materials. The materials have been studied by various scholars and patterns are found. There are two ways to construct a hydrophobic surface: either by using materials with low surface energy, which is the interfacial free energy that quantifies the states of intermolecular bonds, or physically reconstruct the surface to increase its surface roughness, thus promote the total surface area and reduce the contact area between the

liquid and the material. Figure 1 presents the water droplets on two surfaces with different roughness. From the figure, the contact area between the water and the solid surface is much smaller for a rougher surface.

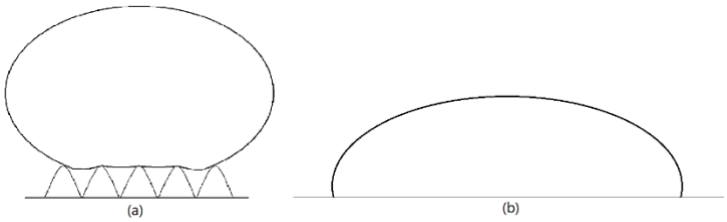

Figure 1. A comparison of water droplets on surfaces with (a) high surface roughness (b) low surface roughness (represented as flat). Notice for the contact area between the water droplet and solid surface, (a) is much smaller than the one of surface (b)

The contact angle (CA) between a droplet and a surface is the most common way of determining whether a surface is hydrophobic or hydrophilic. Refer to Figure 3 for examples of CA. The specific procedure for determining the CA is discussed in the Contact Angle Determination section. If the CA > 90° the surface is considered hydrophobic, whereas if the CA < 90° the surface is considered hydrophilic. Surfaces that are called superhydrophobic have a contact angle between 150° and 180°. Increasing the roughness on a surface is a method of increasing its hydrophobicity. However, it was discovered by Shibuichi *et al.* (1996), who conducted extensive experiments on rough surfaces, that if a flat surface is initially hydrophilic, increasing the roughness and surface area will result in a decrease in the hydrophobicity of the surface. Their experimental research validates the model developed by Cassie and Baxter (1944):

$$cos\theta = R_f f_{SL} cos\theta_0 - f_{LA} \quad (1)$$

where θ is the CA of the surface with roughness, and θ_0 is the CA of the original flat surface. Roughness factor R_f, is defined as the ratio of the total three-dimensional surface area (within a two-dimensional geometric area) to the actual two-dimensional geometric area (if there was no topography). As the roughness of the surface increases the roughness factor would increase. The variables, f_{SL} and f_{LA} represent the fractional flat geometrical areas of the solid-liquid and liquid-

air contact areas between the water droplet and the surface. As shown in Figure 1 (a), while the surface is becoming rougher, the area of solid-liquid interface (f_{SL}) would decrease, and the area of liquid-air (f_{LA}) would increase. Besides, the cosine of the flat contact angle would shift from positive to negative as the flat CA exceeds 90°. Therefore, the roughness factor (R_f) and the fraction areas (f_{SL} and f_{LA}) would affect the CA differently depending on whether the material is initially hydrophobic (contact angle >90°), according to Equation 1. For a hydrophobic surface, this equation describes the fact that increasing roughness on surfaces that are initially hydrophobic will make it more hydrophobic. The relationship is opposite for a hydrophilic surface.

A layer of thin wax covers most plants surfaces. The composition of these layers is similar to paraffin, but also contains a mixture of large hydrocarbon molecules. A pristine and flat paraffin surface *(R_f = 1)* is shown to have a CA of 110° on average (Ray and Bartell 1952). Since the contact angle indicates a hydrophobic surface, the actual plant surface should have a relatively higher contact angle. Researches have shown that microstructures and the surface morphology of the leaves and flower petals were indeed the most significant contributors of hydrophobicity. Several well-known effects of surface morphological features causing the increase of the contact angle are the Lotus Effect, the Taro Effect, the Salvinia Effect, and the Rose Petal Effect. The effects are described in several previous studies (Neinhuis and Barthlott 1997, Nasri *et al.* 2014, Bhushan and Nosonovsky 2010, Bhushan and Jung 2006, Koch *et al.* 2013). We obtain data either through our own experiments or from the published data on previous studies. In this study, I set out to quantify how the dimensions of features on the plant surface affect the hydrophobicity of the surface. I used both experimental data generated within this research as well as data from the literature to come to my conclusions. The results of this research could be used to simulate the hydrophobic surfaces, and 3D printer will be used to do that.

ii. Research Motivation (Personal)

For almost all of the 15 summers in my life, I have been visiting my father's hometown, Shicheng, a small town in the southern part of China. The town is widely known as "the town of lotus." Every time I go there, something interesting intrigues me. Whenever I play with the water and lotus leaves, I inspect the water droplets, like a handful of shiny pearls, roll down the leaves and leave nothing on the surfaces. This phenomenon caught my interest, and I kept thinking of the cause of the "smooth and frictionless" surface. After I got to know some basics of natural science, I thought that a completely smooth surface is unachievable for plants. "But how was the surface frictionless and rough at the same time?" I was confused, so I decided to search for the answer. It turned out that several previous studies have described the surface structure of the leaf as having "hydrophobicity" or "water repellency." Protruding papilla cells lying under a waxy paraffin layer created those properties. Both of them have rough structures and contribute to hydrophobicity together. Knowing the high potential benefit of hydrophobicity to humanity once it can be produced artificially and extensively, I wanted to know what physical characteristic of the surface is the most prominent in promoting the hydrophobicity of the structure. The commercial and industrial values of hydrophobic materials are great motivations for the attempt to develop artificial hydrophobicity. If a desirable value for each surface feature could be obtained from the research, I can probably make a surface that is most hydrophobic. This is my motivation to conduct the research.

iii. Research Question and Hypothesis

Hydrophobic properties are a result of both the composition (paraffin) and morphology (microstructure) of the plant surface (Barthlott and Neinhuis 1996). Since the chemical composition of the surfaces is the same (i.e., a layer of paraffin), this research project will

determine how the surface morphology affects the hydrophobicity or "superhydrophobicity" of the leaf. This study is going to investigate the relationship between certain morphological feature and its effect on hydrophobicity. To achieve this, the water droplet behaviors on plant surfaces are examined, the surface details are looked using microscopic images, and specific features are related to the resulting hydrophobicity.

Before conducting any experiments, I hypothesized that various surface features (e.g., papillae-like cells, hillocks, or bumps on the plant surface) affect the hydrophobicity of a plant surface by increasing its roughness. Such determinable features, such as the height of the papillae-like cells, the interspace distance between each bump, and the full width at half maximum (FWHM or Mid-Width), are shown in Figure 2 below. The Cassie-Baxter Equation is used to predict the trend of variations of the CA as the roughness increases on hydrophobic and hydrophilic surfaces. Setup of the equations is presented in the next section.

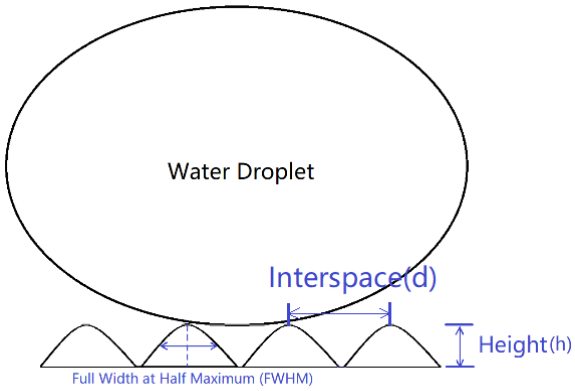

Figure 2. Features of plants surfaces measured using several parameters: Height (h), Interspace (d), Full Width at Half Maximum (FWHM or Mid-Width).

The study determined the CA on paraffin first because of two reasons. It is necessary to know the CA of paraffin since it covers most plant surfaces, and the flat CA is required for the calculation using the Cassie-Baxter Equation (Equation 1). Secondly, the device and procedures used for measuring the CA should be tested for precision before it could be used for obtaining the crucial data. The paraffin CA determination is going to the control experiment, and will also verify the experimental procedures. According to Ray and Barte (1953), the fact that there are different

states of paraffin, such as the crystalline state and the waxy state, does not significantly affect the CA of paraffin. If my setup and procedure can give the same CA as those other studies, the experiment could be used to measure contact angles on actual surfaces of leaves.

After the device and procedures of measuring CA is modified to get reliable results, the experiment proceeds in measuring the CA on surfaces of actual petals. The flower petals are analyzed using a Scanning Electron Microscope (SEM). The pictures are then analyzed to obtain the surface features and characteristics. Combined with data from previous studies, the individual surface morphology data, and CA data will be obtained, and I will make them into a graph with each of them on an axis. The paper compares the graphs with the graphs of the Cassie-Baxter equation mentioned above, and analysis is made. The point of this is to see if there are any trends, and the comparison can give us reliable estimations of the correlations. If, according to the estimation and the actual data trend, a point appears where specific value of a parameter corresponds to the maximum contact angle, the information could be used to create a hydrophobic surface that produces the highest contact angle, which would be the next step of the research - application.

3. Materials and Methods

i. Plant Samples Preparation

Four sets of data come from the experiments conducted by myself, and the rest were obtained from previous studies. Contact angles of paraffin, an orange daisy (*Gerbera* daisy, from the family Asteraceae), a white daisy (*Shasta* Daisy from the family Asteraceae), and a red rose (*Rosa 'Mister Lincoln'*) were analyzed in this study. The origins of the flowers are specified in the appendix. To keep the samples fresh, they are put into water and the petals are sprayed daily. All flower petals in the experiment are cut from fresh stems within a week of separation. Deionized

water washes and cleans the flower petals before experimentation. The petals are cut into squares of 1 cm×1 cm and put into CA and SEM analysis.

ii. Contact Angle Determination

In this part of the experiment, the measurements are taken in a condition of 20±2°. The method used to determine the hydrophobicity of a particular material is by conducting the contact angle measurement, as shown in Figure 3. The contact angle is the inner angle conventionally measured through the liquid, where a macrolevel liquid–air interface meets a solid surface. The figure also shows the contact angle of a hydrophobic surface (above 90°), and the contact angle of a hydrophilic surface (smaller than 90°).

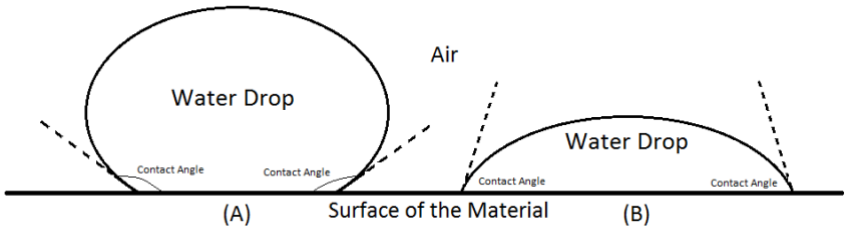

Figure 3. Determining hydrophobicity of different materials using the contact angle. The contact angle is the inner angle conventionally measured through the liquid, where a macrolevel liquid–air interface meets a solid surface, as shown. (A)The contact angle of a hydrophobic surface is above 90 degrees, and a superhydrophobic surface has a contact angle of 150 degrees or more. (B)The contact angle of a hydrophilic surface is smaller than 90 degrees.

To take the high-resolution pictures with water droplets on the surface, a device is made to support the system with strong background light and moderate image amplification. Figure 4 shows the design of our device and its picture. This procedure of measuring the contact angle is based on a previous study by Guillaume Lamour and Ahmed Hamraoui (2010).

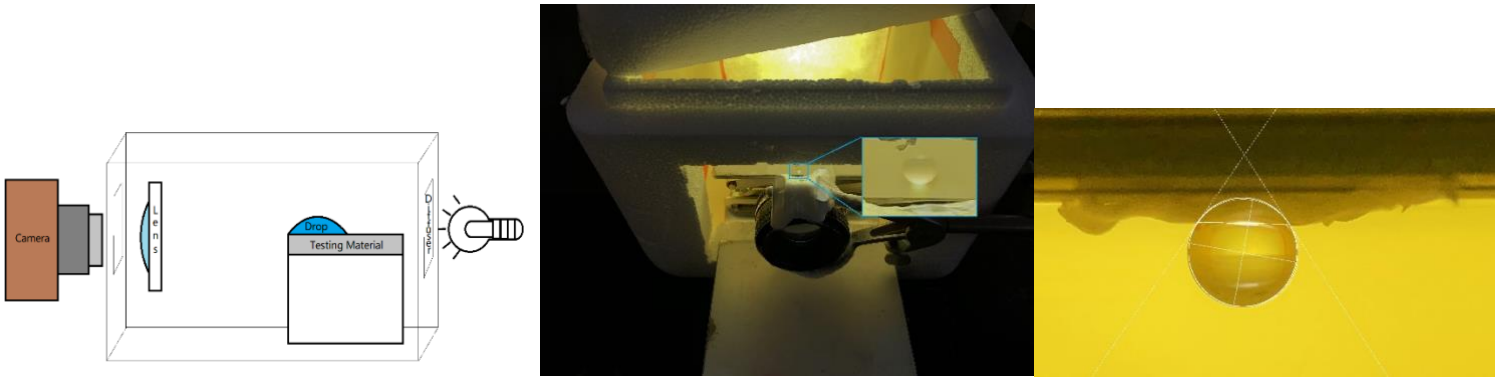

(a) (b) (c)

Figure 4. Contact angle measurement setup. Strong background light passes through a diffuser, and the scene is amplified by the lens, giving a clear image to the camera. (a) shows the setup of the planned setup of the measuring device, and (b) shows the actual device. On Figure 4 (b), the water droplet is emphesized. (c) shows an analyzed water droplet (on surface of a white daisy, *Shasta* Daisy from the family Asteraceae).

Figure 4 shows the setup of the device which is used to determine the CA of the testing material. Information of the light source, the lenses, and the camera used are provided in the appendix. For the first experiment, the material used is the Parafilm M, which is made of paraffin, as for the second part actual plants are used. The pictures taken for samples with water droplets are analyzed with ImageJ (Rasband, 2009), an image analyzing software, and the Contact Angle Plugin for the software (Brugnara, 2006). The program automatically calculates the contact angle for high-resolution pictures with a surface and a water droplet. The analyzed picture is shown in Figure 4. (c). Since the several types of paraffin all have similar contact angles, the contact angle of parafilm is compared to the data from Ray and Barte (1953).

It is after five trials and countless improvements that the image finally gets to a high resolution and the contact angle measurements are approaching the one from the previous studies. The device was re-designed for several times in order to produce a maximum resolution, and to make the sample easier to focus. Specifically, after the second and the third trial new devices are

made with smaller internal space to let the light focus and illuminate the sample. Macro lens is added at the fourth trial and is proved to be very useful. Trial 4 and 5 used the same equipment, but trial 5 adjusted the diffuser to let more light to come in.

For the CA measurement of actual biological surfaces, a new problem arose: the surfaces are not macroscopically flat, so it is hard to determine the baseline of the surface. The parallel vision is not able to obtain the actual baseline. Thus, the CA is controversial. To make sure the CA on all surfaces were comparable, a new method was developed to take the average of 3 sets of measurements, as shown in Figure 5.

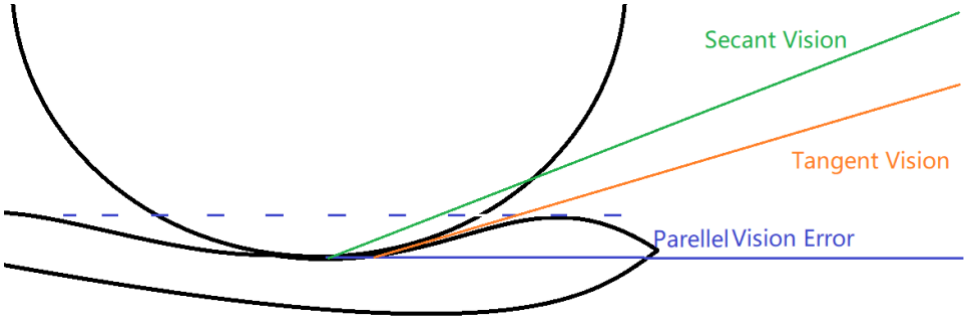

Figure 5. The parallel vision error and two other different visions designed to improve the measurement. This technique is used for measuring the contact angle on plant surfaces.

In Figure 5, the secant vision and the tangent vision are used to obtain the actual baseline and minimize the errors. The method to find the spot to take the tangent vision is to move the camera from the secant vision down until the surface of the plant starts to cover the water droplet. In the experiment, three pictures are taken for each vision. The researcher determines nine respective contact angles, and he takes an average for each experiment on an individual plant.

iii. Analysis of Microstructures

The microstructures of the florets are analyzed using a Scanning Electron Microscope (SEM). The Scanning Electron Microscope used was a Hitachi TM4000 PLUS Tabletop

Microscope. In the research, the plant samples were analyzed in secondary electron mode with an operating voltage of 15 KeV. Only the bottom width and interspace of the papillae were determined from SEM images. The height of the papillae on the samples was not determined because this study did not examine the cross-section of the plants. Those features, as shown in Figure 6, are analyzed using ImageJ processing program (Rasband, 2009). After the analysis of each floret, the results are taken the average and listed in the table in the result section. Figure 6 picks the examples of the orange daisy (*Gerbera* Daisy, from the family Asteraceae) and white daisy (*Shasta* Daisy, from the family Asteraceae).

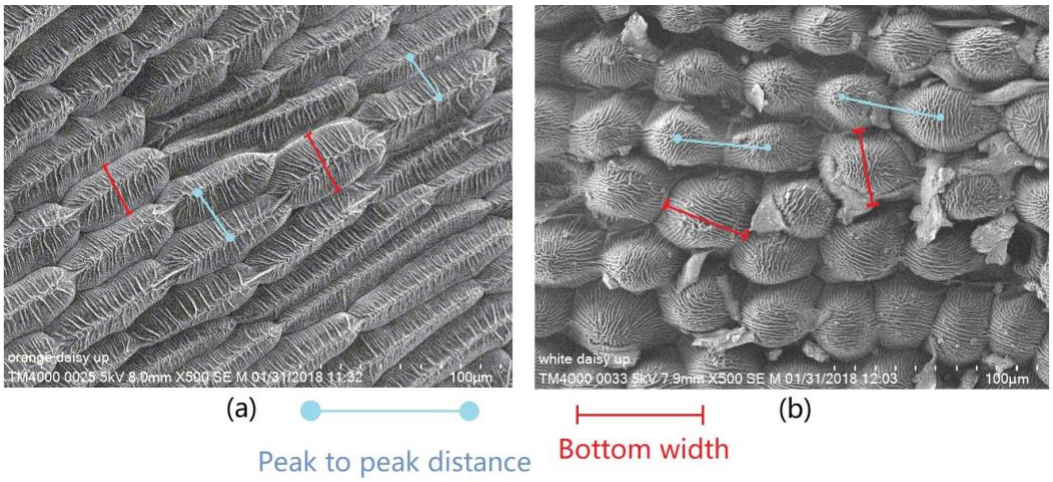

Figure 6. Images taken using SEM showing (a) the surface of orange daisy (*Gerbera* daisy, from the family Asteraceae); (b) the top surface of white daisy (*Shasta* Daisy, from the family Asteraceae). Two of the several measurable parameters (Peak to peak distance and bottom width) are presented in the figure.

Published CA and morphology data sets from the literature were used in order to augment the experimental data. Normalizing the data obtained from various studies is difficult because of different parameters are used in the measurements. One of the most important parameters is the mid-width (or FWHM). Some studies used the bottom-width (width of the elongated epidermal bumps at the bottom), and others used the mid-width (width of the bump at a height equal to half of the peak to minimum height). Some plant surfaces have long strips (shown in Figure

7(A)(B)(C)) while some have circular papillae or hillock cells (Figure 7 (D)). The formation of such strips is due to the elongation of the epidermal cells. The different shapes of the surfaces influence their hydrophobic properties by altering the value of solid-liquid and liquid-air contact fraction, which is included in Equation (1) and is discussed in the Equation Setup section. To get comparable data, the bottom-widths are scaled into the mid-widths. There are four common types of hydrophobic structures on plant surfaces. Those classifications and their images are shown in Figure 7 (Koch *et al.* 2013). Within each type of structure, the patterns are almost the same despite the magnitude of the scale, so for each type, the conversions between bottom-width and mid-width are similar. The method is to identify each structure and use the formula of conversion for the corresponding structure type. The estimated conversions presented on the right of Figure 7 is made based on the cross sections on the left.

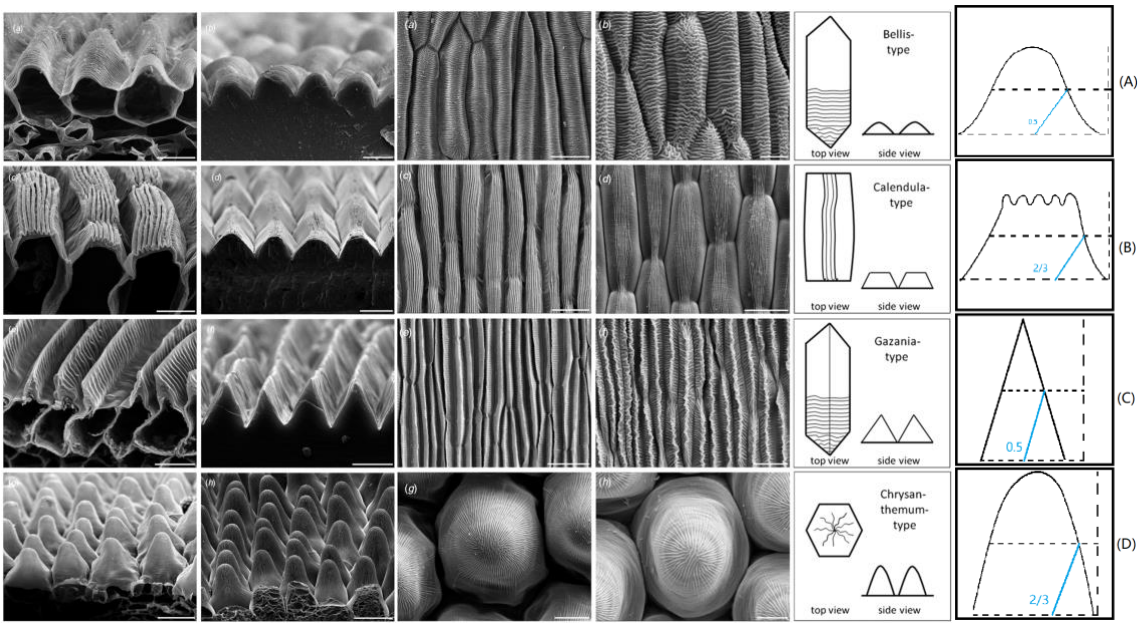

Figure 7. Classifications and characteristics of the four types of structures on plant surfaces. (A)Bellis type (B)Calendula type (C)Gazania type (D)Chrysanthemum type. The top view and the cross-section pictures are published initially in Koch et al. 2013. The right part including the examples of each of them and the conversion factor from the bottom-width to the mid-width was the estimation made by the author basedon the pictures on the left.

The method to convert a data of bottom-width into the mid-width is first to identify which type of structure it is. For instance, the surface of white daisy (Figure 6 (b)) belongs to the Chrysanthemum type. Thus the mid-width of the hillock is two-thirds of its bottom-width. Using this method, all of the bottom-width values were converted into mid-width values.

Notice the difference of Figure 7. (D) from other three types is that it has round, papillae and hillock-like cells while (A), (B) and (C) have elongations of epidermal cells. Their impacts on the prediction would be discussed in the Equation Setup section.

iv. Equation Setup

It is mentioned in the hypothesis part that the relationships between certain parameters are predicted using the Cassie-Baxter equation that is often used for solid-liquid-air contacts. The specific predictions are presented at the end of this section.

It is notable that a number of assumptions are made in the model based on previous data. These assumptions are described in detail in the following section. As for experimenting, the hope is that the mathematical models and the equations match the circumstances in only the range of contact angles and the trend of the curve. As mentioned, before any experimentation, a graph based on the Cassie-Baxter equation is generated. Given the equation:$\theta = R_f f_{SL} cos\theta_0 - 1 + f_{SL}$, there are some variables that still need to be correlated or known. The contact angle of the original flat surface (θ_0) is obtained using the inverse equation (Bhushan and Jung 2006). Those researchers measured the CAs as well as other variables in the equation for various hydrophobic and hydrophilic surfaces, and they concluded that the flat surface of hydrophobic surfaces have CAs of around 105°, similar to the CA of paraffin. Hydrophilic surfaces, in contrast, do not have the cover of the layer of paraffin, thus the flat surfaces have CAs of 85°. Based on their study, two

equations are made for hydrophobic and hydrophilic surfaces with different values of flat contact angle (θ_0). Other values of variables (except for R_f, discussed below) are known.

Since the contact angle (θ) and one of the surface parameters are going to be the dependent and independent variables, respectively, only the roughness factor (R_f), and the fraction of the solid-liquid contact area (f_{SL}) are unknown. It is proposed in the research of Bhushan and Jung (2006) that f_{SL} does not change very much with mid-width in the range of typical papillae mid-width values. A f_{SL} value of 0.5 was used, in accordance with Bhushan and Jung (2006), because the dimensions of the surface features in this study are similar to those in their study. Since f_{LA}=1-f_{SL}, it automatically becomes 50%, as shown in Figure 8.

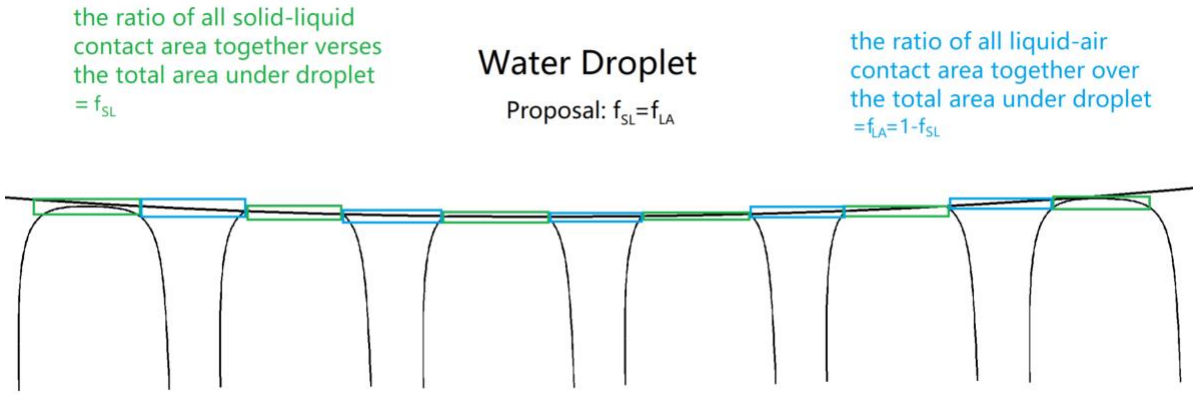

Figure 8. The areas under a water droplet. It is proposed that $f_{SL}=f_{LA}=\frac{1}{2}$. f_{SL}=0.5 is the ratio of the solid-liquid phase over the total distance, and f_{LA} could be expressed as 1-f_{SL}, or 50%.

From Figure 8 we can see that in this cross-section $f_{SL} = f_{LA} = \frac{1}{2}$. The common pattern for hydrophobic surfaces is to have elongated epidermal cells that have solid-liquid-air interfaces in only one direction, as shown in Figure 7 (A)(B)(C). Note that for some hydrophobic surfaces, rather than cells different in bottom-widths and length, the papillae are circular, and the cells are almost equally spaced (Figure 7 (d)). Those papillae have same peak-to-peak distance and radii on both the longitudinal and the lateral directions. The effect of such round papillae could not be

neglected, so two separate equations for hydrophobic surfaces are generated, one using $\frac{1}{4}$ as k (graph shown in Figure 10 (a)) and the other using $\frac{1}{2}$ (Figure 10 (b)).

For the roughness factor, estimation could be made for hydrophobic and hydrophilic surfaces using 3-dimensional microscopic pictures of petals taken by Bhushan and Jung (2006). It is estimated when the when the mid-width is 10 micrometers, the roughness factor is about 2. Since the peak-to-peak distance depends only on the mid-width, as the mid-width gets smaller and approaches 0, the surface become so closely stacked by humps that the real surface area, and consequently the roughness factor, become infinitely large. Similarly, as the mid-width increases, the surface is going to be approaching a perfectly flat surface. Figure 9 shows a mathematical model for the relationship between the mid-width and the roughness factor, and the two asymptotes are shown. The equation is adjusted to fit the condition that 10 micrometers of mid-width corresponds to a roughness factor of 2:

$$R_f = \frac{10+w}{w} \qquad (2)$$

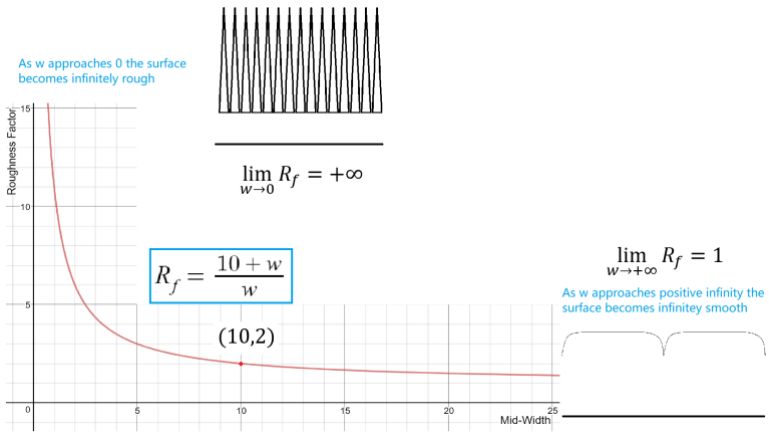

Figure 9. The equation generated to express the relationship between the roughness factor and the mid-width. It is based on a data point, so it is not expected to be as precise. However, it shows the trend and approximately the expected values.

Taking into account the estimations for R_f and S_{SL} described above, equation (1) can be shown as:

For Hydrophobic plant surfaces:

$$CA = cos^{-1}[\frac{1+w}{w} \cdot cos(105°) \cdot (\frac{1}{2})^2 - 1 + (\frac{1}{2})^2] \quad \text{(a).(3)}$$

$$CA = cos^{-1}[\frac{1+w}{w} \cdot cos(105°) \cdot \frac{1}{2} - 1 + \frac{1}{2}] \quad \text{(b).(4)}$$

For Hydrophilic plant surfaces:

$$CA = cos^{-1}[\frac{1+w}{w} \cdot cos(85°) \cdot (\frac{1}{2})^2 - 1 + (\frac{1}{2})^2] \quad \text{(c).(5)}$$

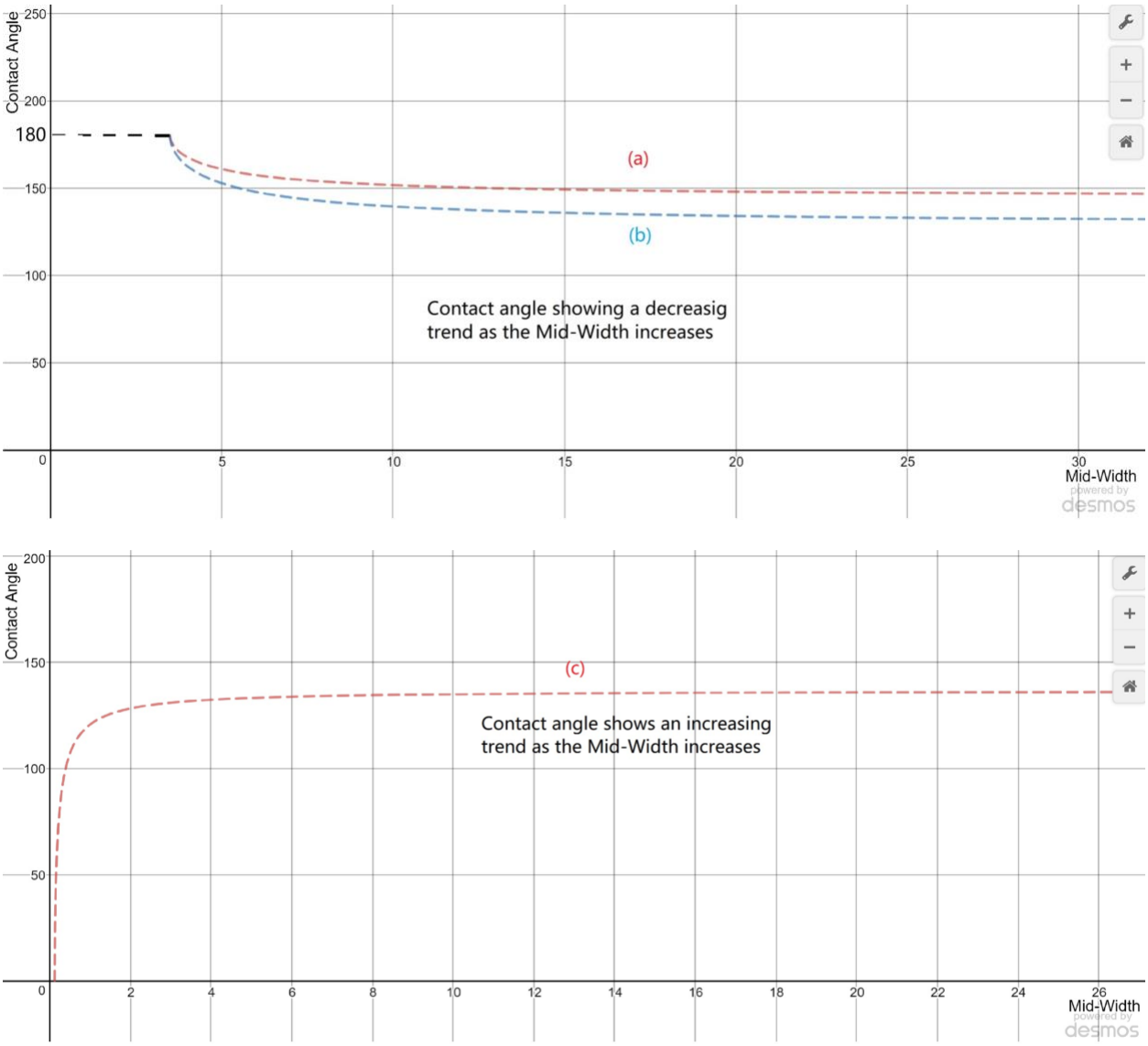

Figure 10. The graphs of the two functions expressing the contact angle on hydrophobic (10 (a), 10 (b).) or hydrophilic (10 (c).) surfaces as functions of the mid-width of the individual papillae. The graphs are powered by desmos graphing calculator, beautiful, free math (Desmos Graphing Calculator, 2018).

The several characteristics and trends found on the graphs of CA as functions of mid-widths (Figure 10.) are in accordance with the trends suggested by the Cassie-Baxter equation. Figure 10 (a) and 10 (b) show the graphs for the two hydrophobic models, while 10 (c) shows the one for the hydrophilic model. The hydrophobic CA function starts its left at 180°, and as the mid-width increases the CA decreases. For the hydrophilic one, the CA increases as mid-width goes up, which is also an expected feature.

The surface morphology data and contact angle data were obtained after the second part of the experiment. Graphs were made with each of them on the x-axis. The point of this was to see if there are any trends in the data. If a trend appears that shows that the CA increases with mid-width, for example, this information could be used in the future to engineer synthetic hydrophobic surfaces for different applications (as discussed later). Because the experiment only provided enough reliable data to show the relationship between the contact angle and the mid-width, this section only describes how the equation for those two variables are produced. Other data graphs are shown in the appendix.

4. Results

i. Paraffin Contact Angle Measurements

The CA measurement method used in the paper has been adjusted for several times and finally validated by similar values on other published studies. Table 1 presents the several good data from the trials.

From the data, we found the average contact angle of both directions on Parafilm M, and compared it to the measurements conducted by Ray and Bartell (1952). The difference between

the two measurements is about 0.02%, indicating that the procedures of this measurement is reliable, and thus could be used to measure the contact angles of plant surfaces.

Name	CA left (°)	CA right (°)	CA average (°)
4-1.	111	114.3	112.6
4-2.	106.2	110.9	108.6
4-3.	108.8	110.9	109.8
4-4.	115.8	114.1	115
4-12.	106.4	107.8	107.1
5-4.	109.6	108.9	109.2
5-7.	112.1	107.5	109.8
5-8.	120.2	114.6	117.4
Average	111.2625	111.125	111.1875

Table 1. The table presents the measurements of CA(both sides) on Parafilm M and the average.

ii. Floret Contact Angle Measurements

With the device presented in Figure 4 and the method proposed in Figure 5, this study measured the contact angles of plants precisely. Similar to the measurements for paraffin, the pictures were analyzed in ImageJ (Rasband, 2009), and the average CAs were determined. Table 2 includes the surface details results of the experiment. The underlined results are data from the experiment.

iii. Microscopy Images and Analysis

The plants are put under the SEM, whose model information are specified in the section of Analysis of Microstructures. Figure 11 shows three of the best pictures taken during the experimentation. The pictures are analyzed using ImageJ (Rasband, 2009) to get the surface factors such as the bottom-width and the peak-to-peak distance. Those parameters are presented along with the CAs in Table 2. Notice that some experimental data in Table 2 come from other sources.

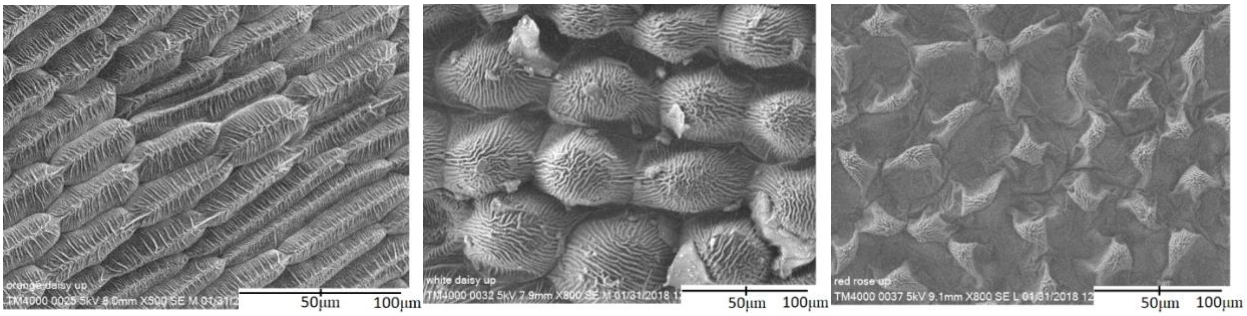

(a) (b) (c)

Figure 11. Three best images of the top side of the flower petals taken using an SEM. (a) orange daisy (*Gerbera* Daisy, from the family Asteraceae). (b) white daisy (*Shasta* Daisy, from the family Asteraceae). (c) red rose (*Rosa 'Mister Lincoln'*).

Classification	Specie Types	Average θ (°)	Bottom-width (μm)	Mid-width(μm)	Diameter (μm)
Hydrophobic (θ_0>90°)	**Bellis perennis**	139.55	15.3	10.2	N/A
	Calendula officinalis	Not Usable*	10.2	6.8	N/A
	Mutisia acuminata	147.75	16.2	8.1	N/A
	Pericallis-Hybride	127.75	32.5	21.67	N/A
	Orange Daisy	144	22.8	13.68	N/A
	White Daisy	131.4	37.7	25.13	N/A
	Fresh Lotus	152.23	N/A	10	6
	Dry Lotus	147.45	N/A	10	8
	Fresh Taro	150.5	N/A	15	10
	Dry Taro	149.14	N/A	15	14
Hydrophilic (θ_0<90°)	*Fresh Fagus*	75.5	N/A	10	30
	Dry Fagus	66.5	N/A	5	20
	Fresh Magnolia	85.3	N/A	13	34
	Dry Magnolia	73.2	N/A	12	30

Table 2. Data obtained from the experiment and other published researches. The sources are labeled with the data set: Underline-own experiment; **Bold**-Koch et al. 2013; *Italic*-Bhushan and Jung 2006. * The data of Calendula officinalis is not usable because its CA changes over a range of 30° depending on the direction of measurement. The variations of contact angles when facing different directions has to do with the nanostructures, which will not be discussed in this research.

Table 2 shows that the mid-width has the largest number of values and is the only variable that shows correlation with CA. Figure 12 shows the graph of the mid-width and contact angle, with the presence of a trend line. For convenience, other graphs of relationships not discussed here are included in the appendix. For the data determined in this experiment, error bars are created using the standard deviation generated for the data obtained in this experiment.

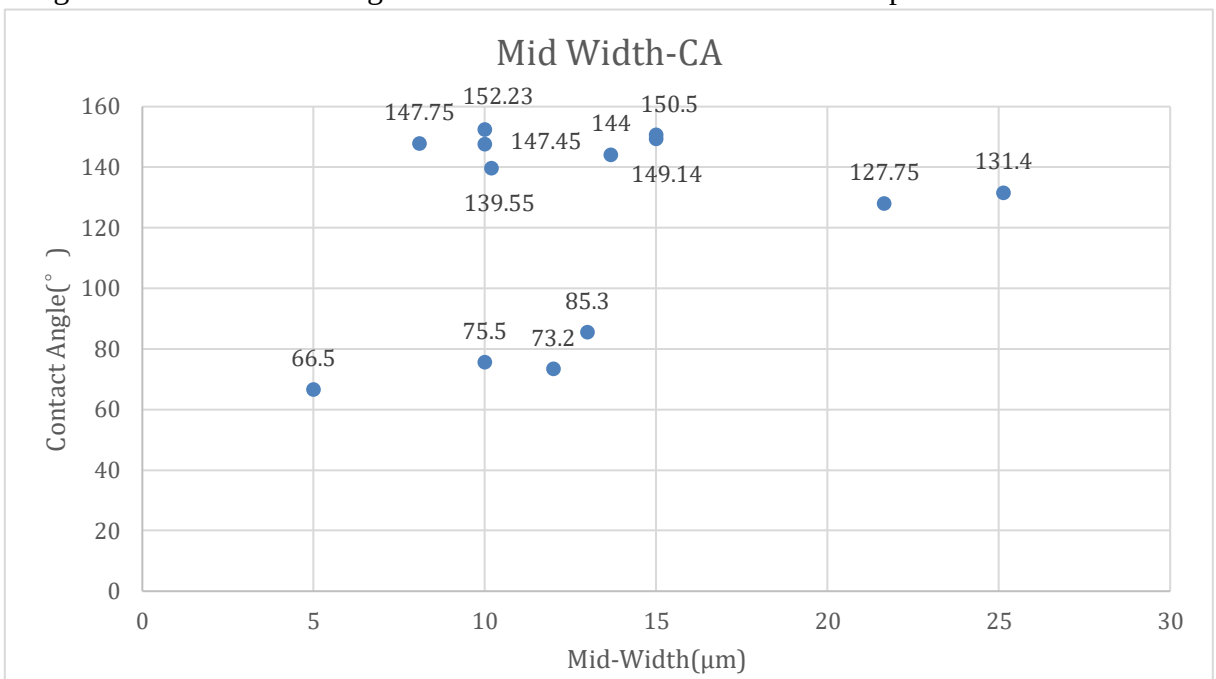

(a)

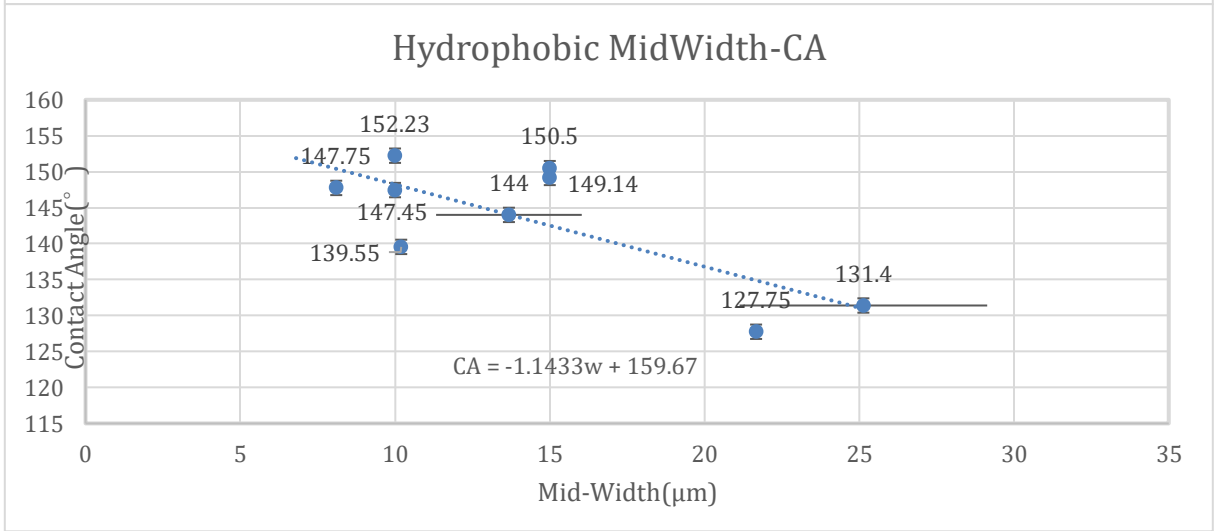

(b)

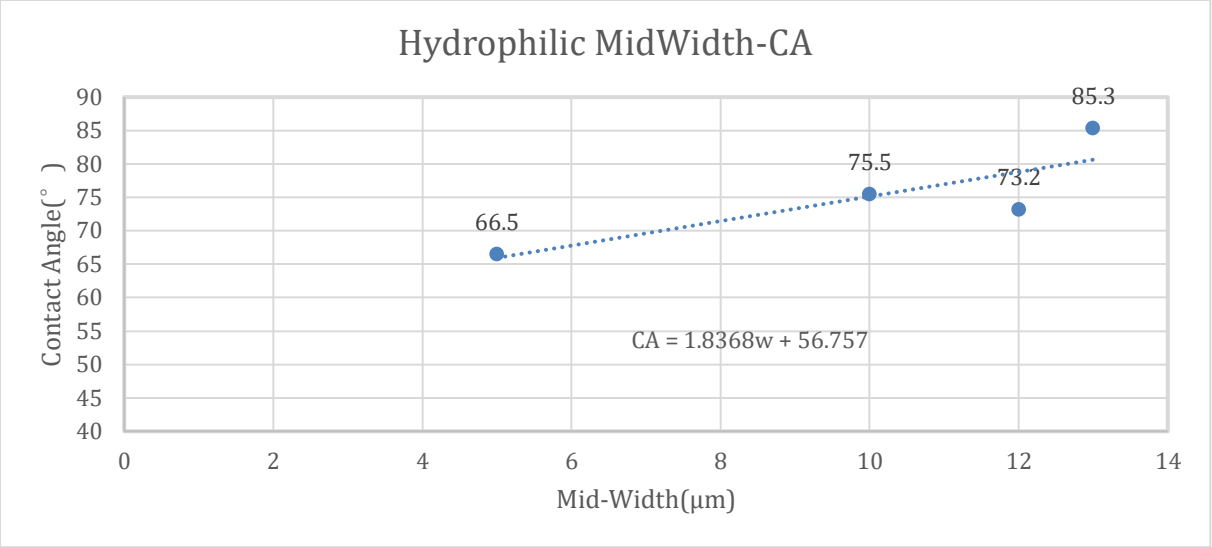

(c)

Figure 12. The graphs of contact angle versus the mid-width. The complete graph (a) explicitly consists of two separate parts. The graph is divided into the hydrophobic graph (b) and the hydrophilic graph (c). In graph (b) and (c) linear trend lines are generated to show the increasing or decreasing trends.

In graph (a) two trends could be seen, thus the graph is separated into hydrophobic (b) and hydrophilic (c). It is clear in graph (b) that the trend of the CA of hydrophobic surfaces is negative as the mid-width increases. Hydrophilic surfaces, in contrast, have positive trends of CA as the mid-width goes up. Hydrophobic surfaces have CAs ranging from 125° to 155°, and hydrophilic plants have CAs from 65° to 85°. In the next section, we will prove whether the hypothesis is true based on a comparison of the trend and the ranging of data points and the hypothesized graphs.

5. Discussion

The equations of the two trend lines obtained from the best fit models are graphed on the set of coordinates for each respective surface types using the Desmos Graphing Calculator (2018). The results for hydrophobic and hydrophilic surfaces are shown in Figure 13 as solid lines (orange) and green dots representing the data points while the predictions are displayed as dotted lines (blue and red).

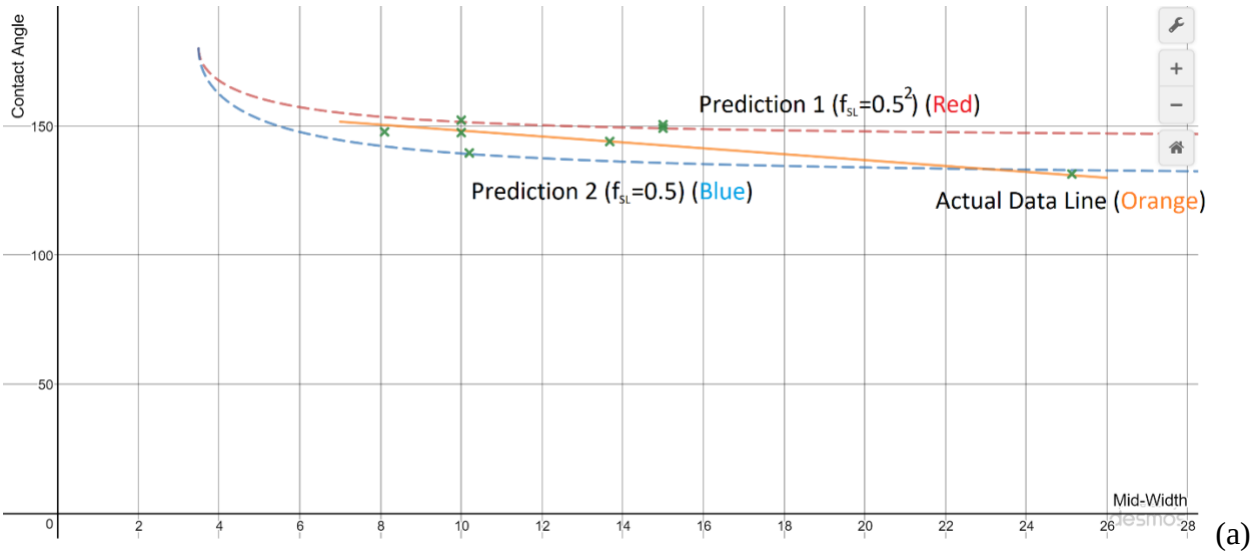

(a)

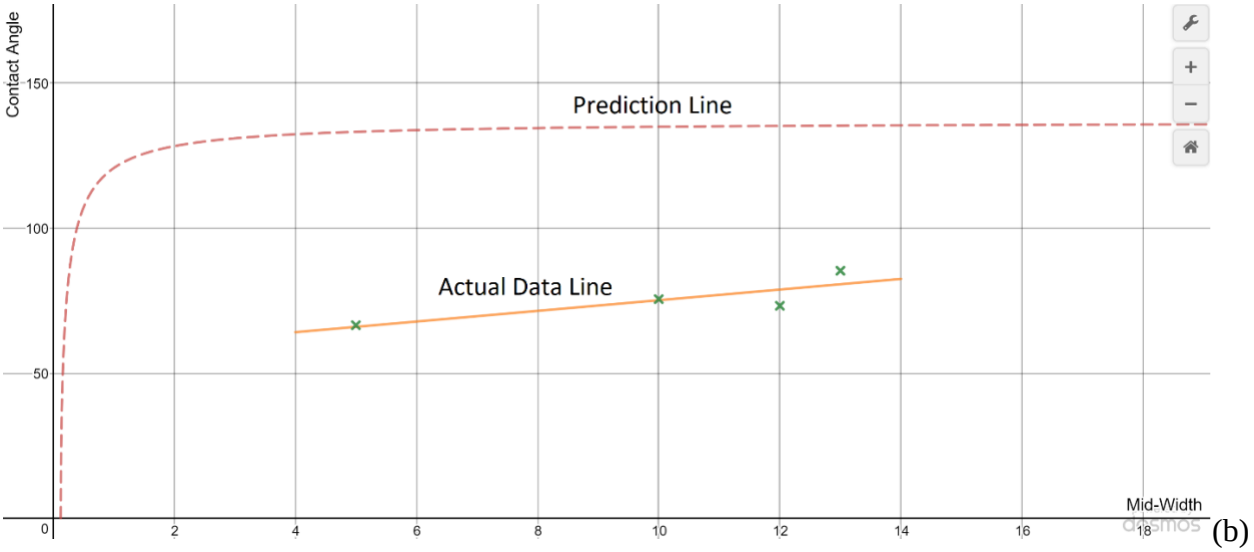

(b)

Figure 13. The predicted and actual results of hydrophobic (a) and hydrophilic (b) surfaces. The actual data lines are displayed as solid lines (orange) and green dots representing each single point while the predictions are displayed as dotted lines (blue and red).

For hydrophobic surfaces, Figure 13 (a) shows that in the data domain and from the standpoint of range of the contact angle, the two prediction lines both have the same trend of decreasing. The figure also shows that some points fall on the prediction 1 line while some fall on the second prediction. Either of the predictions are really close to the measurements. It does not matter much whether the fraction of solid-liquid contact area (f_{SL}) is $\frac{1}{2}$, or $\frac{1}{4}$, because the data points

fall between them. Both predictions are tested by the experiment, and thus can be used for later studies.

For hydrophilic surfaces, Figure 13 (b) exhibits the vast difference between the prediction and the actual data line. Although both lines have the same trend of increasing, the data range of the prediction line is two times the actual line. It is more likely that the data line reflects the actual scenario more because according to the prediction, the contact angle is increased to nearly 150° for a hydrophilic surface. Such increase is impossible because the contact angle of a surface made of hydrophilic materials could never be raised to 150° by promoting roughness, as stated by the Cassie-Baxter equation (Cassie and Baxter 1944).

A new model is required to explain this phenomenon. For this reason, the Wenzel Model of solid-liquid contact is introduced. Different from the Cassie equation, which regards the contact of solid, liquid, and air pockets inside the valleys, the Wenzel model only cares about the contact between solid and liquid. Since the surface is initially hydrophilic, the water droplets will automatically immerse into the papillae valleys on a rough surface. For a hydrophilic surface, this model should be used rather than the Cassie model. The two models and their equations are exhibited in Figure 14 and the two equations below.

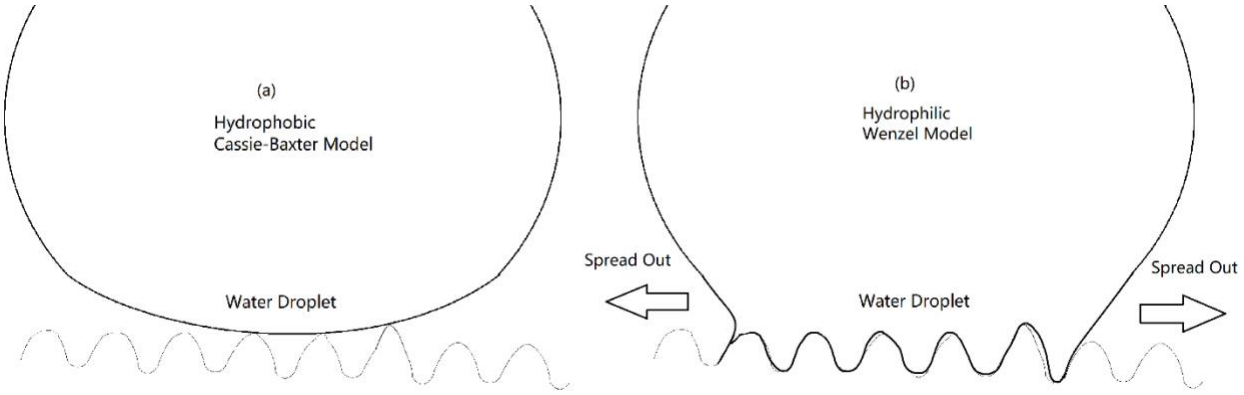

Figure 14. (a) the Cassie-Baxter state of wetting. Water stays outside the sunken spots. (b) the Wenzel state of wetting. Water goes into the valleys because the flat surface is hydrophilic. In this case the liquid-air contact should not be considered, thus the Wenzel equation should be used for a hydrophilic surface.

(a)The Cassie-Baxter Equation: $cos\theta = R_f f_{SL} cos\theta_0 - f_{LA}$ (1)

(b)The Wenzel Equation: $cos\theta = R_f cos\theta_0$ (6)

$$cos\theta = \frac{10+w}{w} cos\theta_0 \quad (7)$$

Equation (1) was the original Cassie-Baxter equation. Equation (6) and (7) use the new Wenzel equation for hydrophilic surfaces. Since the $R_f = \frac{10+w}{w}$ does not change from the Cassie equation to the Wenzel equation, the new model of relationships between CA on a hydrophilic surface and the mid-width of the papillae using the Wenzel equation (Equation (7)) is graphed on the same coordinate as a blue dot line, as shown in Figure 15 below.

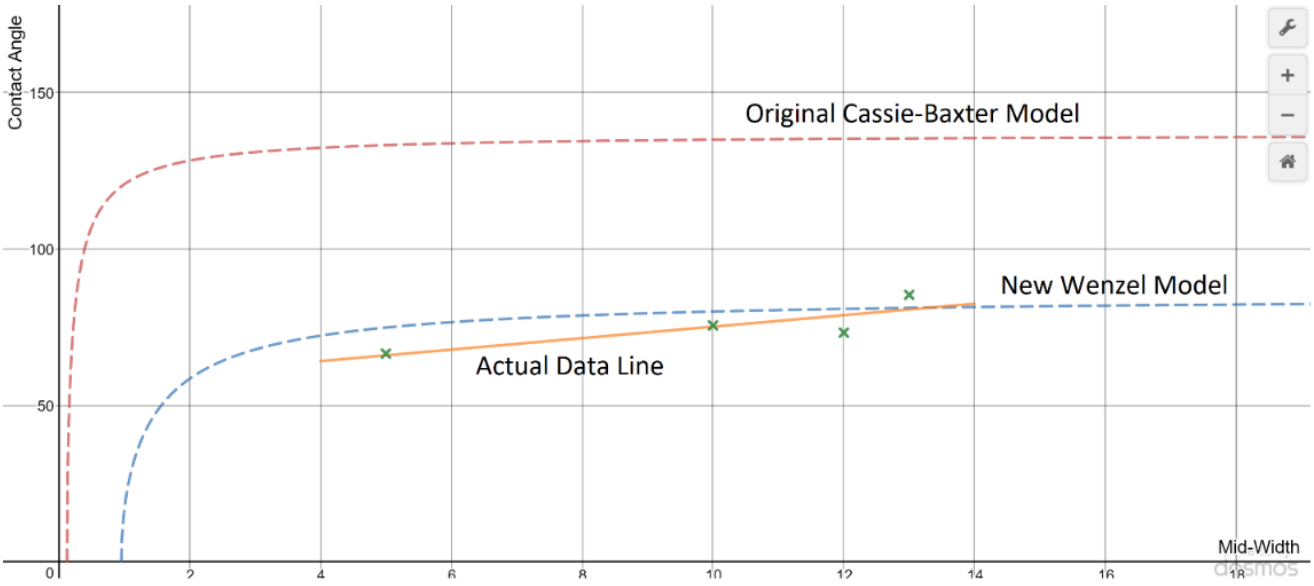

Figure 15. The hydrophilic graph including the new Wenzel model.

It is obvious from the data that the Wenzel model is better at dealing with hydrophilic surfaces than the Cassie-Baxter model. It is close to the data line in both the trend and the contact angle range in the domain. This Wenzel equation could be used for determining the relationship between surface morphologies and contact angles of hydrophilic surfaces.

6. Conclusion and Application

This study analyzed several plant surfaces from different standpoints. The use of several techniques such as CA measurements, SEM imagery, and math models helped the group greatly in the process of quantifying different parameters. This paper investigated the relationship of hydrophobicity, microlevel surface features and the states that a water drop could have on a surface. The study proved that the Cassie-Baxter equation is more useful when dealing with hydrophobic surfaces whereas the Wenzel equation is more effective with hydrophilic surfaces. By using mathematical models, the research predicted and tested the relationship between the contact angle and the mid-width of the papillae. The hypothesis was proved to be partially right, and by revising the model, the researcher found the desirable models to describe the hydrophobic and hydrophilic situations. Those models would be used in later researches to develop the best model for hydrophobicity.

Besides, because the preparation of cross sections of plants involves special procedures so as to not damage microstructure when making the cut, the research does not involve the cross-section imagery. Future studies will involve analyses of cross sections.

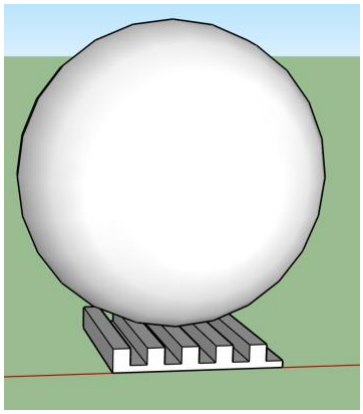

Figure 16. One of the early models developed using the results of the research. By changing the height, the mid-width, the interspace, and the shape of the elongated papillae, the hydrophobicity is going to vary according to models that would be further developed. The software used is SketchUp (3dwarehouse.sketchup.com, 2018)

Once the hydrophobic model is established, and the sample is produced using hydrophobic materials to enhance its hydrophobicity further, it could be used in various industrial and technological applications. The applications of hydrophobic materials include but are not restricted to anti-icing, drag-reduction, reversible surfaces, self-cleaning, anti-fogging, rain wares, sensing, and separation. The experiment requires further investigation because better mathematical models could be developed based on data. The researcher expects better results and trends if more data are to be gathered. This requires more data from both experimentation and the published articles. The researcher is going to conduct several more experiments to get more set of data, thus get a more accurate trend line. With all the parameters examined in the experiment, the author has already started the plan to use a 3D printer to mimic the hydrophobic surfaces in microlevels. Figure 16 shows one of the developed models. The future of this direction of the research looks promising.

7. Appendix

i. Specific information of the devices used

The flower petals that are analyzed are from Barnie's Flower Shop Inc, specifically in 616 Allegheny River Blvd. Oakmont, PA 15139. The phone number is 412-88-7411, and the website is www.berniesflowershop.net. Thanks to the lady in the flower shop, she gives the flower for the research for free, "because it is for science."

The parafilm was the standard Parafilm M, a plastic paraffin film with a paper backing produced by Bemis NA.

In the contact angle measurement experiment, a light source, a diffuser, a set of lenses, and a camera are used. The models of those are listed below:

The diffuser is one sheet of normal yellow paper.

Light Source: Bright Effects CFL Bulbs. 13W, 120VAC, 60Hz, 200mA. UL #E170906.

Lenses: Nikkor, Nikon. 50mm, 1:1.8, 3262181. Inverted.

Camera: Apple iPhone 8, using the default software and default settings.

ii. Other Data

The following paragraph shows other data graphs (i.e., Height and the Aspect Ratio of Mid-Widths and Heights). Those graphs exhibit little or almost no trends, a lot of them are a scatter of data. They are graphed but not analyzed or compared with math models.

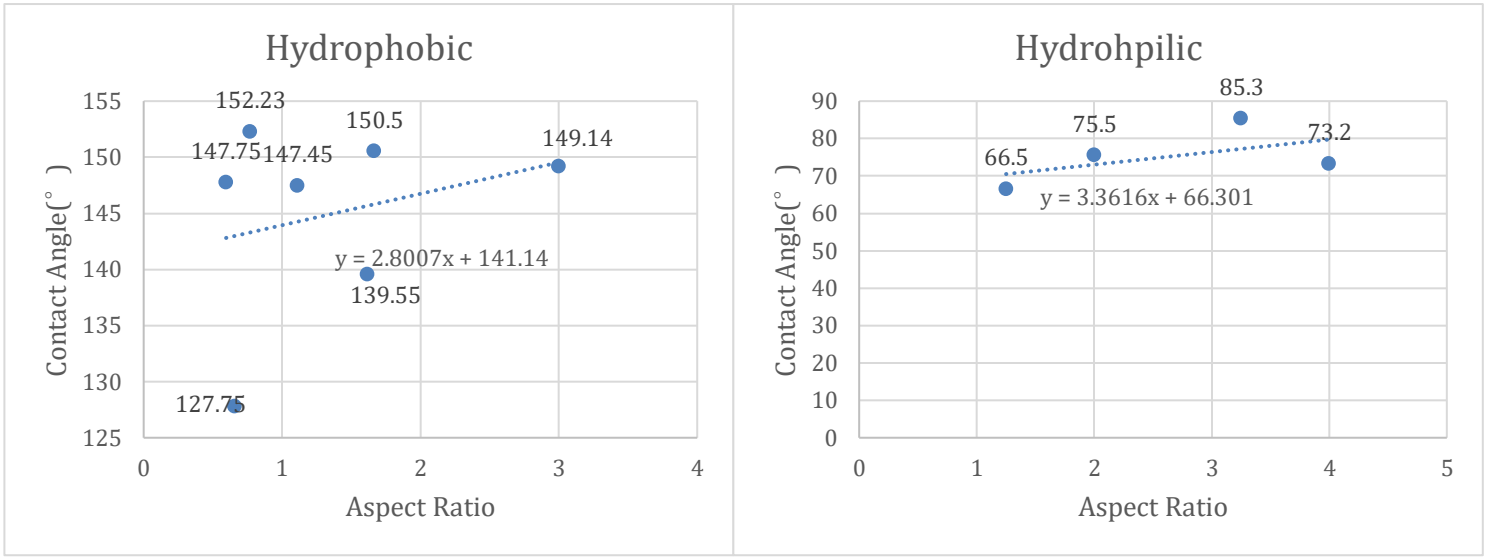

(a) (b)

Figure 17. The graphs of Aspect Ratio (the ratio of Mid-Widths over Heights) on the x-axis verses CA on the y-axis. (a) for hydrophobic surfaces; (b) for hydrophilic plants.

In Figure 17 the width the trend lines show the relationship between Aspect Ratio and CA. The data shows little trends for hydrophobic surfaces (a). it seems like the data points are scattered around randomly. Figure 18 shows the graphs for Height and CA.

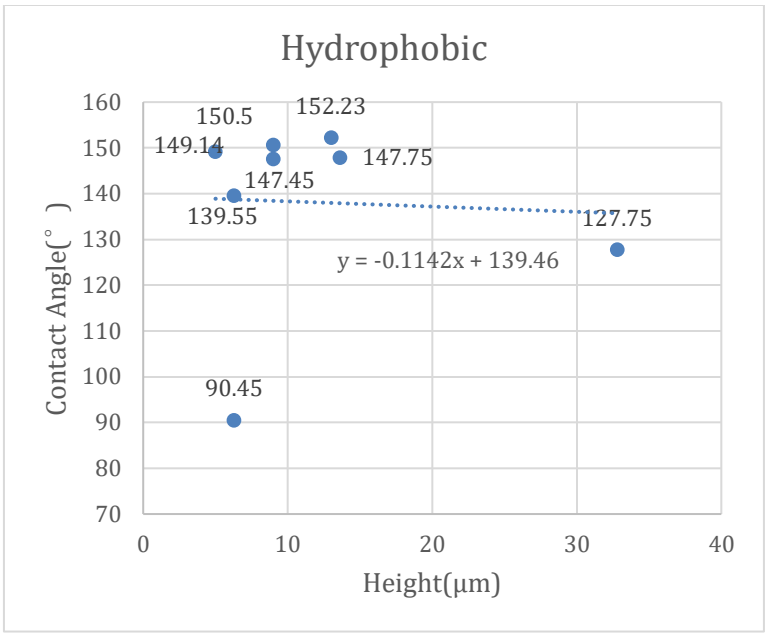

(a)

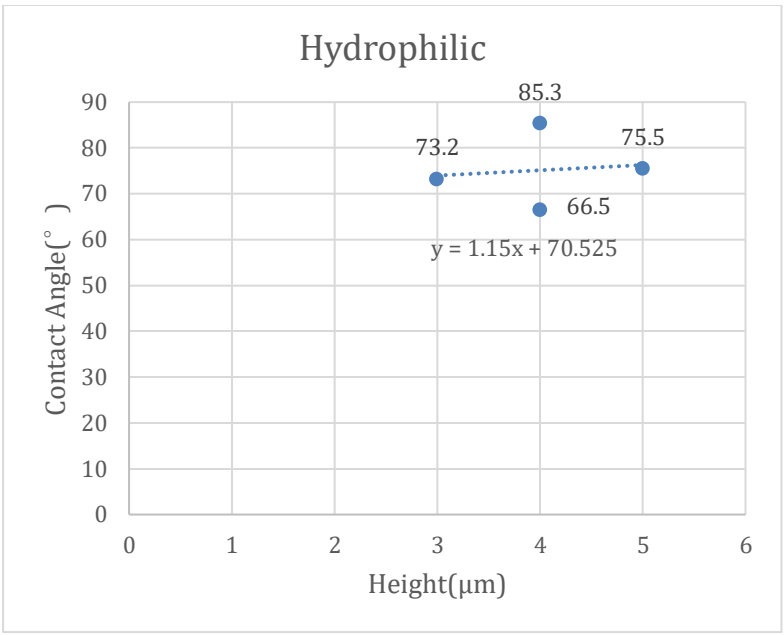

(b)

Figure 18. The relationship between Height of the papillae or epidermal cells and their CA, (a) for hydrophobic surfaces; (b) for hydrophilic surfaces.

This figure shows the relationship between Height of the hillocks or epidermal cells and its CA. There are no apparent trends for the hydrophilic surfaces, and as for the hydrophobic ones the relationship is expressed using the trend line with its equation on the graph. From the equation the slope of this trend line is almost zero, showing that the CA does not vary too much as the height of the bumps changes. This relationship is rather not useful for this paper because the relationship could not be used for hydrophobic surface biomimicry. For the reasons above, those graphs are put in the appendix and not compared with respective predictions.

iii. Acknowledgements

Acknowledgements to Liz Carter and Evan Slow from Angstrom Scientific Inc. for assisting me with taking images.

Thanks to my science research advisor. He offered great help while I was struggling to improve and trying to decide what step I should make. Without his help, there was no way I was able to finish and present this fantastic research. Also, thanks to the teachers in the science department who helped me finding materials for experimentation and those who offered me occasional but generous help.

9. Bibliography

Barthlott W. and Neinhuis C. (1997) Purity of the Sacred Lotus, or Escape from Contamination in Biological Surfaces. *Planta.* **202** 1-8

Bhushan, Bharat and Nosonovsky, Michael (2010) The rose petal effect and the modes of superhydrophobicity. *Philosophical Transactions.* Series A, Mathematical, physical, and engineering sciences. **368**. 4713-28.

Bhushan, Bharat and Yong Chae Jung (2006) Micro- and nanoscale characterization of hydrophobic and hydrophilic leaf surfaces. *Nanotechnology* **17** 2758

Brugnara, M. (2006) Contact Angle (6th ed., Version 2006.12.07) [Computer program]. Retrieved from https://imagej.nih.gov/ij/plugins/contact-angle.html

Cassie, A. and Baxter, S. (1944) Wettability of porous surfaces. *Trans. Faraday Soc.* **40** 546-51

Desmos Graphing Calculator. (2018). Desmos Graphing Calculator. [online] Available at: https://www.desmos.com/calculator [Accessed 24, February. 2018].

Koch, Kerstin *et al.* (2013) Surface microstructures of daisy florets (Asteraceae) and characterization of their anisotropic wetting. *Bioinspir. Biomim.* **8** 036005

Lamour, Guillaume and Hamraoui, Ahmed (2010) Contact Angle Measurements Using a Simplified Experimental Setup. *American Chemical Society and Division of Chemical Education, Inc*. **87**, 1403-1407.

Nasri, N. S. *et al.* (2014) Hydrophobicity Characterization of Bio-Wax Derived from Taro Leaf for Surface Coating Applications. *Advanced Materials Research*. Vol. 104

Rasband, W. (2009) Image J (Version 1.42) [Computer software]. Retrieved from http://rsbweb.nih.gov/ij/index.html

Ray, B. and Bartell. F. (1952) Hysteresis of Contact Angle of Water on Paraffin. Effect of Surface Roughness and of Purity of Paraffin. *Journal of Colloid Science.* **8** 1953-2

Shibuichi, S., Onda, T., Satoh, N. and Tsujii, K. (1996) Super-water-repellent surfaces resulting from fractional structure. *J. Phys. Chem.* **100** 19512-7

@Last Software. (2018) Sketchup Pro 2018 (Version 2018) [Computer software on CD-ROM]. Trimble. Retrieved from https://www.sketchup.com/download/all. Accessed February 25, 2018.